RSC Advances

PAPER

View Article Online
View Journal | View Issue

Cite this: *RSC Adv.*, 2014, **4**, 39984

A rhodamine derivative as a highly sensitive chemosensor for iron(III)†

Kaitian Wu,[a] Hongde Xiao,[a] Lele Wang,[b] Gui Yin,*[ac] Yiwu Quan[a] and Ruiyong Wang*[b]

Received 31st May 2014
Accepted 14th August 2014

DOI: 10.1039/c4ra05180g

www.rsc.org/advances

A novel rhodamine-based fluorescent probe **P1** was synthesized for the optical detection of Fe^{3+}. Compared with other commonly coexisting metal ions in aqueous system, it exhibited high sensitivity and selectivity for Fe^{3+}. The detection limit was only 0.1 μM with fluorescence experiment. The rapid enhancement of fluorescence intensity on the addition of Fe^{3+} provided a good method for the detection for Fe^{3+}. The color change was visible and distinct, so it could be used for naked-eye detection. Furthermore, the fluorescent probe was proved effective when used for detecting Fe^{3+} in living cells and zebrafish. This showed its values in biological aspects.

1. Introduction

Metal ions play important roles not only in chemical reactions but also in a lot of biological processes. They are indispensable in our daily life.[1,2] As a result, it is necessary to find efficient ways to detect different ions selectively and sensitively. Fluorescent probes have been designed and synthesized to meet the above acquirements.[3–5] Fluorescent chemosensors now are widely used in medical, environmental, and biological applications.[6,7] They can show scientists the molecular details of biological processes involved in the change of metal ions.[8,9] Chemosensors can make it possible for remote measurement, hence avoiding the risk of damaging the samples or the need to remove them from their natural medium.[10] For the above reasons, the development of selective and sensitive chemosensors has drawn a great deal of attention.[11]

As one of the most essential trace elements in biological systems, iron plays an indispensable role in the growth and development of living systems, as well as in many cellular biochemical processes.[12] It provides the oxygen carrying capacity of heme around the body. It is also crucial in cellular metabolism and enzymatic reactions.[13] Given its importance in living systems, its deficiency, but also its overdose, can induce serious biological disorders.[14] Iron deficiency will lead to anemia, low blood pressure, and hypoimmunity, because of the difficulties this causes in oxygen delivery to the cells. Conversely, the overloading of iron in living systems can result in reactive oxygen species (ROS) being formed through Fenton reaction. As a result, the lipids, nucleic acids, and proteins can be greatly damaged.[15] Several diseases, such as such as Alzheimer's, Huntington's, and Parkinson's diseases, have already been proved to be connected with cellular toxicity.[16–18] Thus, reliable methods of quantification detection are badly needed in the clinical, medicinal, environmental, and industrial fields.[19] Because of the easy monitoring, low cost, high sensitivity, good selectivity, high level of biosecurity, and rapid enhancement of the fluorescence intensity, chemosensors are a good choice to detect Fe^{3+}, and have made great contributions to the development of fluorescent detection for Fe^{3+} in the past few decades. As we know, rhodamine with a spirolactam structure is colorless and nonfluorescent, whereas ring-opening of the spirolactam induced by an analyte gives rise to a pink color and a strong fluorescence emission. Moreover, rhodamine has a long emission wavelength and high fluorescence quantum yield, which is suitable for detecting ions in living cells. So far, a number of fluorescent probes for Fe^{3+} have been reported,[20,21] but only a few of them are truly satisfactory. Other transition-metal ions, such as Cu^{2+}, Co^{2+}, Cr^{3+}, Pb^{2+}, Hg^{2+}, can easily interfere with the Fe^{3+}, resulting in bad selectivity and sensitivity.[22] Many of the probes cannot be used in living cells because of their cellular toxicity. Furthermore, most of the probes are prone to being influenced by the background fluorescence, because they have a shorter emission wavelength (below 500 nm). Moreover, color change cannot be identified by the naked eye, either,[23–25] and many of them are not compatible with aqueous environments, thus restricting their applications in live applications.[11]

In this work, we developed and synthesized a fluorescent probe **P1** based-on rhodamine. It has high sensitivity and selectivity, and the enhancement of the fluorescent intensity is rapid. It is also compatible with aqueous environments. Strong

[a]State Key Laboratory of Analytical Chemistry for Life Science, School of Chemistry and Chemical Engineering, Nanjing University, Nanjing 210093, People's Republic of China. E-mail: yingui@nju.edu.cn

[b]State Key Laboratory of Pharmaceutical Biotechnology, School of Life Science, Nanjing University, Nanjing, 210093, People's Republic of China. E-mail: wangry@nju.edu.cn

[c]Jiangsu, Key Laboratory of Advanced Catalytic Materials and Technology, Changzhou University, 213164, China

† Electronic supplementary information (ESI) available. See DOI: 10.1039/c4ra05180g

yellow fluorescence can be observed under excitation at 557 nm. Furthermore, the color changes from yellow to deep pink quickly and clearly, after adding Fe^{3+} in **P1**. In the fluorescence titration experiments, the fluorescence intensity remained unchanged even after the concentration of the Fe^{3+} was more than 1 equiv. Moreover, the biological experiment proves that **P1** could perform in living cells, showing its potential for use in practical and a wide range of applications.

2. Experimental

2.1. Materials and apparatus

All of the chemicals were from commercial suppliers. The solvents (methanol, ethanol) were dried and distilled before use. All of the other chemicals were of analytical reagent grade, unless otherwise stated. As for the aqueous solutions, the water was purified by a Milli-Q Advantage Water Purification System. ^{1}H NMR and ^{13}C-NMR spectra were recorded using a Bruker Ultrashield 300 MHz spectrometer operating at 300 and 75 MHz, respectively. Samples were in deuterated dimethyl sulphoxide (DMSO-d_6) as the solvent. Chemical shifts were expressed in ppm, and TMS was the internal standard. Mass spectroscopy was carried out by Micromass GC-TOF and Agilent Technologies 6540 UHD Accurate-Mass Q-TOF LC/MS instruments. An Hitachi Fluorescence spectrophotometer-F-4600 was used to measure the fluorescence spectra. A Varian Cary 50 Probe UV/Vis spectrophotometer was used to measure UV/Vis spectra. An Olympus FV-1000 laser scanning confocal fluorescence microscope was used to capture the fluorescent images.

2.2. Intermediates and monomer synthesis

The overall synthetic steps for the monomer are shown in Scheme 1.

Synthesis of compound a. Compound **a** was synthesized according to an earlier reported article.[26]

Synthesis of compound b. Into rhodamine B (4.79 g, 10 mmol) in ethanol solution (30 mL) in a 100 mL round-bottomed flask was added ethylenediamine (10 mL). The solution was heated at reflux and stirred for 4 h. After cooling to room temperature, a red solid precipitated resulted and was washed by cool ethanol until the filtrate turned colorless.^{1}H-NMR (300 MHz, DMSO, 25 °C): δ = 7.75 (s, 1H), 7.47 (s, 2H), 6.98 (s, 1H), 6.33 (d, 6H, J = 9.0 Hz), 3.31 (d, 8H, J = 6.0 Hz), 2.94 (d, 2H, J = 9.0 Hz), 2.18 (d, 2H, J = 6.0 Hz), 1.07 (t, 12H, J = 6.0 Hz) ESI-MS: m/z = 485.20 $[M + H]^+$.

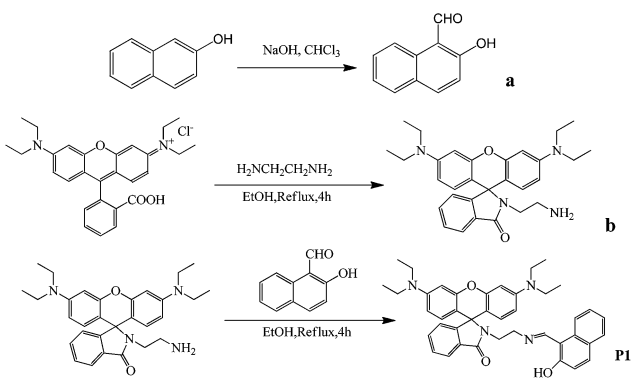

Scheme 1 Schematic of P1 synthesis.

Synthesis of compound P1. Into compound **b** (1.21 g, 2.5 mmol) in ethanol solution (25 mL) in a 100 mL round-bottomed flask was added compound **a** (0.43 g, 2.5 mmol). The solution was then heated at reflux overnight. After cooling to room temperature, a yellow solid precipitated out. The solid was washed by cool ethanol until the filtrate turned colorless, then dried *in vacuo*. Yield: 1.12 g (70%), yellow powder **P1**. ^{1}H-NMR (300 MHz, DMSO, 25 °C): δ = 13.84 (s, 1H), 8.75 (d, 1H, J = 8.5 Hz), 7.38–7.90 (m, 6H), 7.16 (s, 1H), 7.01 (s, 1H), 6.69 (d, 2H, J = 9.2 Hz), 6.29 (dd, 5H, J = 6.0, 6.0 Hz), 3.42 (s, 4H), 3.22 (d, 8H, J = 5.7 Hz), 1.02 (s, 12H) ppm. ^{13}C-NMR (75 MHz, DMSO, 25 °C): δ = 176.42, 167.99, 159.71, 153.94, 153.08, 148.83, 137.21, 134.49, 133.29, 130.57, 129.28, 128.78, 128.65, 128.21, 125.80, 125.42, 124.09, 122.90, 122.64, 118.81, 108.62, 106.59, 105.19, 97.70, 64.64, 49.70, 44.08, 40.99, 12.79 ppm. ESI-MS: m/z = 639.30 $[M + H]^+$ 661.30 $[M + Na]^+$ 677.25 $[M + K]^+$.

2.3. Measurement procedures

Stock solutions of 1.0×10^{-3} M **P1** and 1.0×10^{-3} M Fe^{3+} were prepared by dissolving **P1** in ethanol–H_2O (1 : 1) solution and $Fe_2(SO_4)_3 \cdot 9H_2O$ in double-distilled water, respectively. The Fe^{3+} solution was diluted stepwise to yield working solutions with concentrations ranging from 0.1 μM to 5 μM. The pH range solutions were prepared by adjusting 50 mM Tris–HCl solution with HCl or NaOH solution. Solutions of the other metal ions were prepared by dissolving $Al(NO_3)_3 \cdot H_2O$, $LiClO_4$, NaCl, KCl, $MgCl_2$, $CaCl_2$, $Fe(NO_3)_2 \cdot 6H_2O$, $FeCl_3 \cdot 6H_2O$, $CoCl_2 \cdot 6H_2O$, $Ni(NO_3)_2 \cdot 6H_2O$, $AgBF_4$, $Cr(NO_3)_3 \cdot 9H_2O$, $Cd(NO_3)_2 \cdot 4H_2O$, $ZnCl_2$, $Hg(ClO_4)_2 \cdot 3H_2O$, $CuCl_2 \cdot 2H_2O$, $Pb(NO_3)_2$, $Mn(NO_3)_2$, $GaCl_3$, $FeSO_4 \cdot 7H_2O$, and $HgCl_2$ in double-distilled water (1.0×10^{-3} μM).

2.4. Cell imaging

A fresh stock of HeLa cells was seeded into a glass bottom dish with the density of 1×10^{-5} cells per dish, and incubated for 24 h. Then, 10 μM compound **P1** (198 mL DMEM mixed with 2 mL of 1.0×10^{-3} M **P1** solution in ethanol–H_2O) solution was added to the cells, and then they were incubated for 15 min at room temperature. Then the solution was removed and the cells were washed by PBS (2 mL, three times) to clear any remaining **P1** molecules that did not get inside the cells. Afterwards, 10 μM Fe^{3+} DMEM solution was added to the cells, and then the cells were incubated for 15 min at room temperature. The solution was removed and the cells were washed by PBS (2 mL, three times). Fluorescence imaging was performed with a confocal laser scanning microscopy (λ_{ex} = 546 nm, fluorescent signals were collected at 550–650 nm). The images were captured by a photomultiplier.

2.5. Fluorescent imaging of Fe^{3+} in zebrafish

Zebrafish were raised at 28 °C and maintained at optimal breeding conditions. For mating, male and female zebrafish were maintained in one tank at 28 °C on a 12 h light/12 h dark

cycle, and then the spawning of eggs was triggered by giving light stimulation in the morning. Almost all the eggs were fertilized immediately. All stages of the zebrafish were maintained in E3 embryo media (15 mM NaCl, 0.5 mM KCl, 1 mM $MgSO_4$, 1 mM $CaCl_2$, 0.15 mM KH_2PO_4, 0.05 mM Na_2HPO_4, 0.7 mM $NaHCO_3$, and 5–10% methylene blue; pH 7.5). For the imaging experiments, five-day-old zebrafish were incubated with 10 μM BAN solution for 20 min at room temperature. The solution was then removed, and the cells were washed with PBS (2 mL, three times) to clear BAN molecules attached to the surface of the zebrafish. Afterward, the zebrafish were incubated for 20 min with 40 μM $FeCl_3$ DMEM solution at room temperature. The culture medium was removed, and the treated cells were rinsed three times with PBS (2 mL, three times) before observation. The treated zebrafish were imaged by confocal microscopy. All experiments were performed in compliance with the Regulations for the Administration of Affairs Concerning Experimental Animals published by Bureau of Legislative Affairs of the State Council of the People's Republic of China and guidelines of State Key Laboratory of Pharmaceutical Biotechnology in Nanjing University, and in addition, the institutional committee(s) approved the experiments.

3. Results and discussion

3.1. Fluorescence and visible light response of compound P1 to different metal ions

Various metal ions (Fe^{3+}, Ag^{+}, Al^{3+}, Ca^{2+}, Cd^{2+}, Co^{2+}, Cu^{2+}, Cr^{3+}, Fe^{2+}, Ga^{3+}, Hg^{2+}, K^{+}, Li^{+}, Mg^{2+}, Mn^{2+}, Na^{+}, Ni^{+}, Pb^{2+}, and Zn^{2+}) were used to evaluate the metal-ion bonding property and selectivity of the probe **P1** in aqueous solution. When 10 equiv. of these metal ions were added to 50 μM ethanol–Tris–HCl buffer (v/v, 1/9, pH = 7.0) solutions of **P1**, the Fe^{3+} and Hg^{2+} induced a color change from yellow to pink, but the color change that Hg^{2+} causes was very weak (Fig. 1). With a hand-held UV lamp (at an excitation 365 nm), we could see that both Fe^{3+} and Hg^{2+} induced fluorescence enhancement, but Hg^{2+} only caused a very weak fluorescence enhancement (Fig. 2). Compared to Fe^{3+} and Hg^{2+}, other ions could not cause a color change or fluorescence change.

Fig. 3 shows the UV-Vis absorption spectra of **P1** upon the addition of the various metal ions. The results show that the color change was distinct after adding Fe^{3+} into **P1**. Although Hg^{2+} could induce a color change, the color change was not as obvious as Fe^{3+}.

Fig. 4 shows the fluorescence spectra of **P1** upon the addition of the various ions. **P1** showed no fluorescence upon excitation at 557 nm. Fe^{3+} induced a great increase in the fluorescence intensity. One emission peak at 581.5 nm could be detected. Hg^{2+} also induced an increase in the fluorescence intensity, with an emission peak at 587 nm, but the fluorescence intensity was far weaker than Fe^{3+}. Hence, the 5 nm red shift of the emission peaks between Fe^{3+} and Hg^{2+} and the different

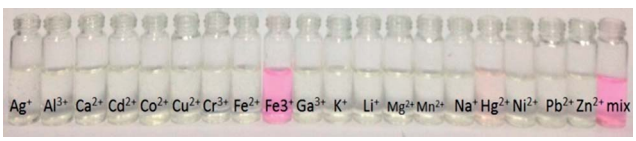

Fig. 1 Changes in the visible light of **P1** (50 μM) in ethanol–Tris–HCl buffer (v/v, 1/9, pH = 7.0) solutions upon the addition of various metal ions (10 equiv.). Mix means **P1** with various metal ions.

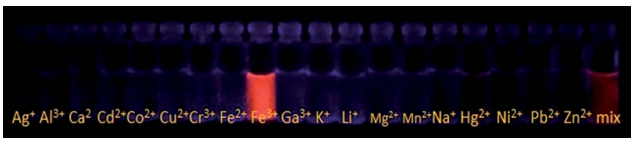

Fig. 2 Changes in the fluorescence of **P1** (50 μM) in ethanol–Tris–HCl buffer (v/v, 1/9, pH = 7.0) solutions upon the addition of various metal ions (10 equiv.) under excitation at 365 nm (with a hand-held UV lamp). Mix means **P1** with various metal ions.

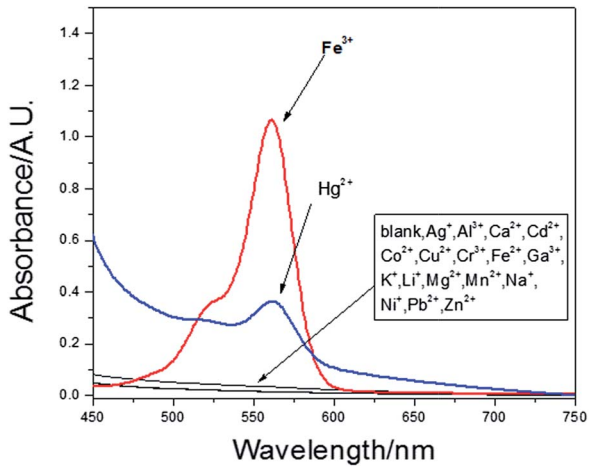

Fig. 3 Absorption spectra of **P1** (100 μM) in ethanol–Tris–HCl buffer (v/v, 1/9, pH = 7.0) with the presence of 1 equiv. of different metal ions.

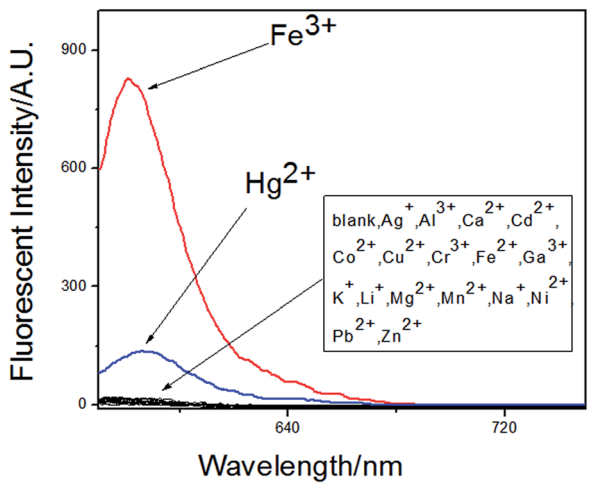

Fig. 4 Fluorescence spectra of **P1** (5 μM) in ethanol–Tris–HCl buffer (v/v, 1/9, pH = 7.0) with the presence of 1 equiv. of different metal ions upon excitation at 557 nm.

fluorescence intensity changes make it possible for the **P1** to discriminate between Fe^{3+} and Hg^{2+}.

3.2. Competition experiment

To prove that the selectivity for Fe^{3+} is good in a complex background of all kinds of metal ions, the fluorescence intensity enhancement of **P1** with Fe^{3+} was detected in the presence of potentially competing metal ions. One equiv. of Fe^{3+} was added into **P1** in the presence of the various metal ions (K^+, Na^+, Ca^{2+} were 50 equiv., whereas the others were 10 equiv.). From Fig. 5, we can see that the fluorescence intensity enhancement caused by Fe^{3+} stayed unchanged after adding all the other kinds of metal ions. Even 10 equiv. of Hg^{2+} could not influence the detection of Fe^{3+}. The phenomenon that even 50 equiv. of K^+, Na^+, Ca^{2+} could not influence the fluorescence intensity enhancement proves that the **P1** probe may perform well in living cells, where the ions K^+, Na^+, and Ca^{2+} are active.

3.3. UV-Vis measurement

Fig. 6 shows the quantitative UV-Vis absorption spectra of **P1**. Different concentrations of Fe^{3+} from 0.1–1 equiv. were added into 100 μM of **P1** in ethanol–Tris–HCl buffer (v/v, 1/9, pH = 7.0) solution. The absorption increased with the concentrations of Fe^{3+} and the pink color became deeper, which could be ascribed to a structure variation of **P1** from a spirocyclic form to a ring-opened amide form.

The molar absorptivity was calculated to be 1.05×10^4 L mol^{-1} cm^{-1}. From the absorption titrations, the association constant of **P1** with Fe^{3+} was calculated to be 9.31×10^{-5} ($R = 0.9998$), using a nonlinear least-square analysis (Fig. 7). This experiment proved that the detection limit of Fe^{3+} is 1.7 μM.

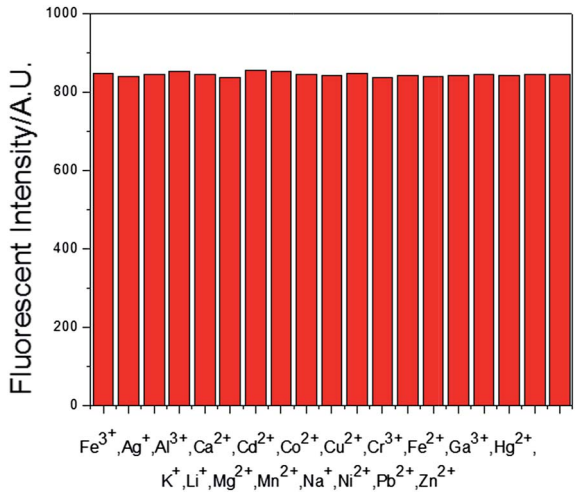

Fig. 5 Competition experiments of **P1** toward Fe^{3+} (1 equiv.) in the absence or presence of various metal ions (K^+, Na^+, Ca^{2+} were 50 equiv., others were 10 equiv.). Excitation wavelength was 557 nm, emission wavelength was 581.5 nm.

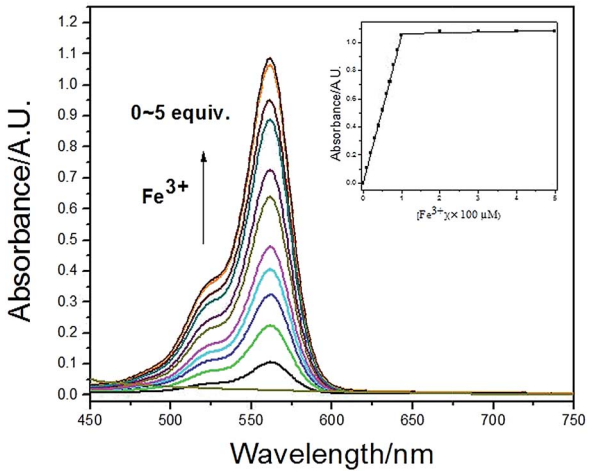

Fig. 6 Absorption spectra of **P1** (100 μM) in ethanol–Tris–HCl buffer (v/v, 1/9, pH = 7.0) solution in the presence of different concentrations of Fe^{3+} (0, 0.1, 0.2, 0.3, 0.4, 0.5, 0.6, 0.7, 0.8, 0.9, 1.0 equiv.).

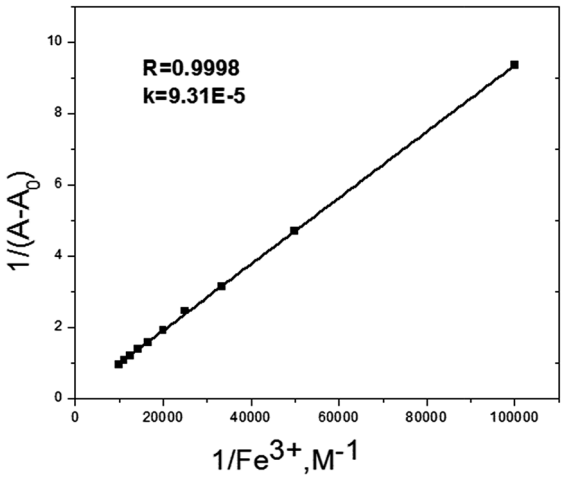

Fig. 7 The association constant of **P1** to Fe^{3+} in ethanol–Tris–HCl buffer (v/v, 1/9, pH = 7.0) solution. The concentration of **P1** was kept at 100 μM.

3.4. Fluorescence measurement

Fig. 8 shows the quantitative fluorescence spectra of **P1** on the addition of different concentrations of Fe^{3+} from 0–5 equiv. in ethanol–Tris–HCl buffer (v/v, 1/9, pH = 7.0) solution. With the increase in the concentration of Fe^{3+}, the fluorescence intensity increased proportionally. When the concentration of Fe^{3+} increased up to 1 equiv. of **P1**, the fluorescence intensity stayed unchanged.

Fig. 9 shows the detection limit of the **P1** probe with Fe^{3+}. The concentration of **P1** was 1 μM and the concentrations of Fe^{3+} increased from 0–1 equiv. of **P1**. This experiment proved that the detection limit of Fe^{3+} is 0.1 μM.

3.5. pH effect

To examine the application of the **P1** probe, the effect of pH experiment was tested. As shown in Fig. 10, the **P1** probe

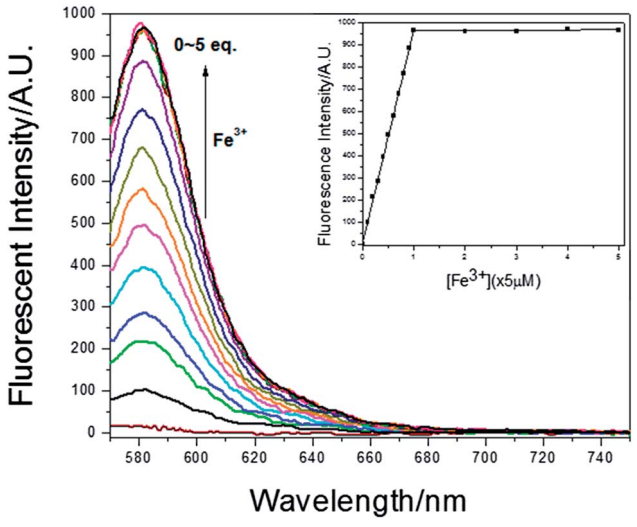

Fig. 8 Fluorescence spectra of **P1** (5 μM) in ethanol–Tris–HCl buffer (v/v, 1/9, pH = 7.0) solution in the presence of different concentrations of Fe^{3+} (0, 0.1, 0.2, 0.3, 0.4, 0.5, 0.6, 0.7, 0.8, 0.9, 1.0, 1.5, 2.0, 2.5, 3.0, 4.0, 5.0 equiv.) upon excitation at 557 nm. Insert: fluorescence intensity changes at 581.5 nm.

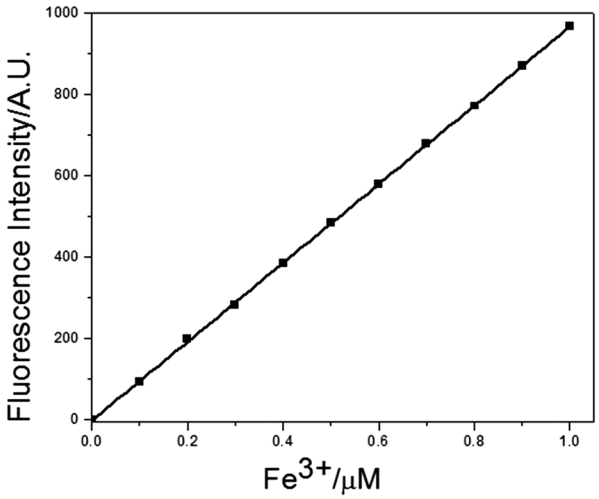

Fig. 9 Fluorescence intensities at 581.5 nm of **P1** (1 μM) in ethanol–Tris–HCl buffer (v/v, 1/9, pH = 7.0) solution as a function of [Fe^{3+}]. The excitation wavelength was 557 nm and the observed wavelength was 581.5 nm.

exhibited no fluorescence in the solution of 2–12 pH. The fluorescence intensity of **P1** in the presence of 1 equiv. Fe^{3+} in a strongly acidic environment was not as strong as in a weakly acidic environment. The fluorescence intensity increased from pH 3–4. A portion of **P1** might decompose in a strongly acidic environment. With a pH range of 4–7, the fluorescence intensity stayed strongest and unchanged. But as the alkalinity increased, the fluorescence intensity decreased rapidly because Fe^{3+} existed in the form of $Fe(OH)_3$, decreasing the quantity of Fe^{3+} in solution. The fluorescence could not be detected when the pH was put up to 7.5. Another experiment was conducted to prove that the disappearance of the fluorescence was caused by the

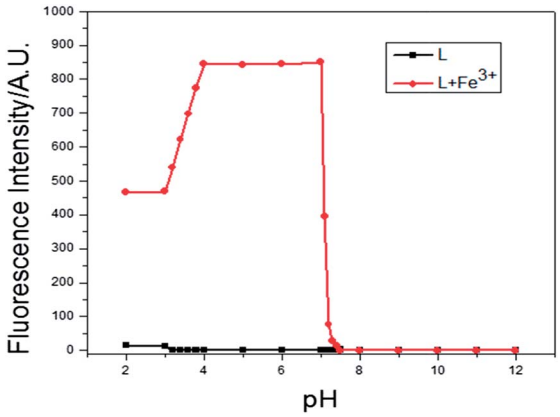

Fig. 10 Fluorescence intensity of **P1** (5 μM) at various pH values in ethanol–Tris–HCl buffer (v/v, 1/9, pH = 7.0) solution, in the absence and presence of Fe^{3+} (1 equiv.). Excitation wavelength was 557 nm, emission wavelength was 581.5 nm.

existence of $Fe(OH)_3$. **P1** was kept in solution (pH = 7.2 and 12.0) for 24 hours, and no new compound was detected by the way of thin-layer chromatography (TLC).[27] That proved that the **P1** probe was stable in alkaline conditions and that the existence of $Fe(OH)_3$ made the fluorescence intensity decrease rapidly.

3.6. Investigation of the binding mode

A Job plot experiment was carried out to study the binding stoichiometry between Fe^{3+} and **P1**. In this experiment, the total concentration of **P1** and Fe^{3+} was kept unchanged at 10 μM, while the concentration of Fe^{3+} increased from 0 μM to 10 μM (Fig. 11). The fluorescence intensity became strongest when the molar fraction of Fe^{3+} was 0.5, which implied that the binding stoichiometry between Fe^{3+} and **P1** is 1 : 1. In addition, in the ESI-MS spectrum of **P1** in the presence of Fe^{3+} (Fig. S1†), the peak was at 725.25 (calculated value was 725.28), which was assigned to [**P1** + Fe^{3+} + CH_3OH − $2H^+$]$^+$. That confirmed the

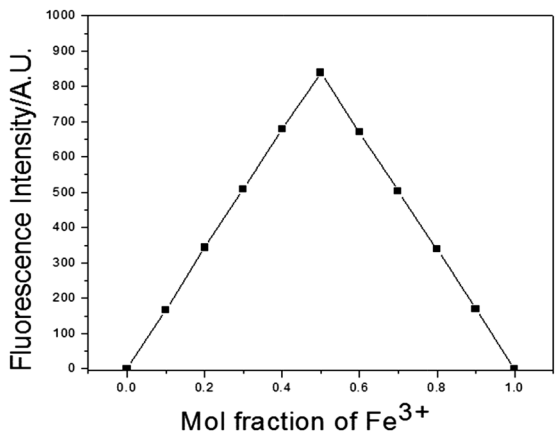

Fig. 11 Job plot of the **P1**–Fe^{3+} complexes in ethanol–Tris–HCl buffer (v/v, 1/9, pH = 7.0) solution, keeping the total concentration of **P1** and Fe^{3+} at 10 μM. The observed wavelength was 581.5 nm.

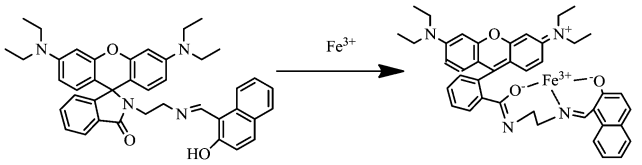

Scheme 2 Proposed mechanism for the fluorescence changes of **P1** on the addition of Fe^{3+}.

1 : 1 stoichiometry for the **P1**–Fe^{3+} complex. The proposed structure of the **P1**–Fe^{3+} complex is shown in Scheme 2.[21] The binding mechanism of **P1** and Fe^{3+} was further investigated by FT-IR spectroscopy (Fig. S7†). The results show the comparison of the FT-IR spectra of **P1** and **P1** + Fe^{3+}, and the characteristic absorption peak of C=O with $\lambda_{max} = 1688\ cm^{-1}$ in the central spirolactam of **P1** disappears and shifts to $1637\ cm^{-1}$ after the addition of Fe^{3+}, indicating that the oxygen atom in the carbonyl group does participate in the coordination. In addition, signals in the region of 1000–1500 cm^{-1} assigned to stretching vibration C–N and C–O moved to high frequency. This could be attributed to coordination of the nitrogen and oxygen atoms.

3.7. Imaging of intracellular Fe^{3+}

When HeLa cells were incubated with **P1** (10 μM) for 15 min at room temperature, nearly no fluorescence could be observed (Fig. 12a). After the treated cells were incubated with Fe^{3+} (10 μM) in the culture medium for 15 min at room temperature, a bright red fluorescence could be observed in the HeLa cells (Fig. 12d). The cell morphology remained in good condition after **P1** got inside the cells, indicating a good cytocompatibility and low toxicity of the probe. As a result, the probe should be applicable for the detection of Fe^{3+} inside living cells.

3.8. Detecting Fe^{3+} in living zebrafish

We further employed **P1** in imaging Fe^{3+} in living zebrafish. As shown in Fig. 13, five-day-old zebrafish, treated with probe BAN (10 μM) for 20 min at room temperature, showed very weak fluorescence (Fig. 13a). Moreover, the **P1**-loaded zebrafish treated with 40 μM Fe^{3+} gave a strong green fluorescence (Fig. 13d). These *in vivo* studies indicated that the **P1** probe is suited for monitoring the distribution of Fe^{3+} in living bodies.

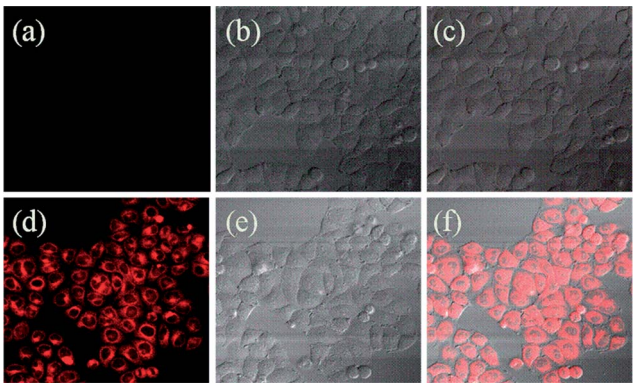

Fig. 12 Confocal fluorescence and bright field images of HeLa cells: (a) fluorescent image, (b) bright field image, and (c) merged image of HeLa cells incubated with the **P1** (10 μM) for 15 min. (d) Fluorescent image, (e) bright field image, and (f) merged image of HeLa cells incubated with Fe^{3+} (10 μM) for 20 min after treating with **P1** ($\lambda_{ex} = 546$ nm, fluorescent signals were collected at 550–650 nm).

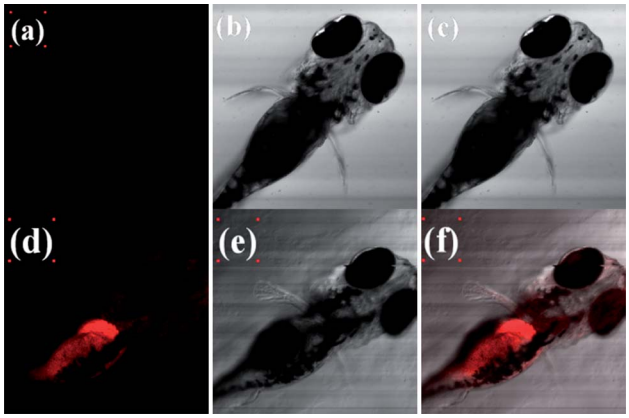

Fig. 13 Fluorescence images of Fe^{3+} in zebrafish using the **P1** probe upon excitation at 546 nm. (a) Fluorescent image, (b) bright field image, and (c) merged image of zebrafish incubated with the **P1** probe (20 μM) for 40 min. (d) Fluorescent image, (e) bright field image, and (f) merged image of **P1**-loaded zebrafish incubated with Fe^{3+} (40 μM) for 40 min.

4. Conclusions

In conclusion, we designed and synthesized a new rhodamine-based compound **P1**. It was highly sensitive and selective for Fe^{3+}. It had fluorescence enhancement and the color change was visible after adding Fe^{3+}. The excitation wavelength was 557 nm and the emission wavelength was 581.5 nm. The detection limit of the **P1** probe with Fe^{3+} was 0.1 μM, which showed its good sensitivity. Experiments for cell imaging proved its good cytocompatibility and low toxicity, which meant it is suitable for the detection of Fe^{3+} inside living cells.

Acknowledgements

We thank the National Natural Science Foundation of China (no. 21174061), National Basic Research Program of China (no. 2014CB846004), Jiangsu Key Laboratory of Advanced Catalytic Materials and Technology (no. BM2012110) and Jiangsu Province Science Technology Innovation and Achievements Transformation Special Fund (BY2012149).

References

1 B. Valeur and I. Leray, *Coord. Chem. Rev.*, 1999, **205**, 7–14.
2 Q. Maa, X. Zhang and X. Zhao, *Anal. Chim. Acta*, 2010, **663**, 85–87.
3 M. Vonlanthen and N. Finney, *J. Org. Chem.*, 2013, **78**, 3980–3985.
4 V. A. Babain1, A. V. Legin and D. O. Kirsanov, *Radiochim. Acta*, 2009, **97**, 479–484.

5 H. Hisamoto, H. Tohma and T. Yamada, *Anal. Chim. Acta*, 1998, **373**, 271–273.
6 Z. Li, K. Li and H. Zhan, *Biochem. Eng. J.*, 2012, **11**, 2–10.
7 H. N. Kim, M. H. Lee and H. J. Kim, *Chem. Soc. Rev.*, 2008, **37**, 1465–1472.
8 D. P. Kennedy, C. D. Incarvito and S. C. Burdette, *Inorg. Chem.*, 2010, **49**, 916–923.
9 H. Wang, D. Wang and Q. Wang, *Org. Biomol. Chem.*, 2010, **8**, 1017–1026.
10 M. H. Noir and B. Dureault, *Sens. Actuators, B*, 1995, **29**, 386–391.
11 K. Moon, Y. Yang, S. Ji and J. Tae, *Tetrahedron Lett.*, 2010, **51**, 3290–3293.
12 R. R. Crichton, D. T. Dexter and R. J. Ward, *Coord. Chem. Rev.*, 2008, 1189–1199.
13 C. Li, C. Zou and Y. Li, *Dyes Pigm.*, 2014, **104**, 110–115.
14 J. Wang, D. Zhang, Y. Liua and P. Dinga, *Sens. Actuators, B*, 2014, **191**, 344–350.
15 P. Xie, F. Guo, R. Xia and Y. Wang, *J. Lumin.*, 2014, **145**, 849–854.
16 J. R. Burdo and J. R. Connor, *BioMetals*, 2003, **16**, 63–75.
17 J. An, Z. Yang, M. Yan and T. Li, *J. Lumin.*, 2013, **139**, 79–83.
18 A. S. Pithadia and M. H. Lim, *Curr. Opin. Chem. Biol.*, 2012, **16**, 67–73.
19 X. Chen, S. Wua, J. Han and S. Han, *Bioorg. Med. Chem. Lett.*, 2013, **23**, 5295–5299.
20 N. R. Chereddy, K. Suman, P. S. Korrapati, S. Thennarasu and A. B. Mandal, *Dyes Pigm.*, 2012, **95**, 606–613.
21 J. H. Huang, Y. F. Xu and X. H. Qian, *Dalton Trans.*, 2014, 5983–5989.
22 H. Li, L. Li and B. Yin, *Inorg. Chem. Commun.*, 2014, **42**, 1–4.
23 L. Yang, W. Zhu, M. Fang, Q. Zhang and C. Li, *Spectrochim. Acta, Part A*, 2013, **209**, 168–192.
24 P. Danjoua, L. Lyskawa, F. Delattre and M. Becuwe, *Sens. Actuators, B*, 2012, **171**, 1022–1028.
25 L. Wang, H. Li and D. Cao, *Sens. Actuators, B*, 2013, **181**, 749–755.
26 L. Jiang, L. Wang, B. Zhang, G. Yin and R. Wang, *Eur. J. Inorg. Chem.*, 2010, 4438–4443.
27 H. Xiao, K. Chen, N. Jiang, D. Cui, G. Yin, J. Wang and R. Wang, *Analyst*, 2014, **139**, 1980–1986.